

1 **Spatial radionuclide deposition data from the 60 km radial area around the**  
2 **Chernobyl nuclear power plant: results from a sampling survey in 1987**

3  
4 Valery Kashparov<sup>1,3</sup>, Sviatoslav Levchuk<sup>1</sup>, Marina Zhurba<sup>1</sup>, Valentyn Protsak<sup>1</sup>, Nicholas A.  
5 Beresford<sup>2</sup>, and Jacqueline S. Chaplow<sup>2</sup>

6  
7 <sup>1</sup> Ukrainian Institute of Agricultural Radiology of National University of Life and Environmental Sciences of  
8 Ukraine, Mashinobudivnykiv str.7, Chabany, Kyiv region, 08162 Ukraine

9 <sup>2</sup> UK Centre for Ecology & Hydrology, Lancaster Environment Centre, Library Avenue, Bailrigg, Lancaster,  
10 LA1 4AP, UK

11 <sup>3</sup> CERAD CoE Environmental Radioactivity/Department of Environmental Sciences, Norwegian University of  
12 Life Sciences, 1432 Aas, Norway

13 *Correspondence to:* Jacqueline S. Chaplow ([jgar@ceh.ac.uk](mailto:jgar@ceh.ac.uk))

14 **Abstract.** The data set “Spatial radionuclide deposition data from the 60 radial km area around the  
15 Chernobyl nuclear power plant: results from a sampling survey in 1987” is the latest in a series of data  
16 to be published by the Environmental Information Data Centre (EIDC) describing samples collected  
17 and analysed following the Chernobyl nuclear power plant accident in 1986. The data result from a  
18 survey carried out by the Ukrainian Institute of Agricultural Radiology (UIAR) in April and May  
19 1987 and include sample site information, dose rate, radionuclide (zirconium-95, niobium-95,  
20 ruthenium-106, caesium-134, caesium-137 and cerium-144) deposition, and exchangeable  
21 (determined following 1M NH<sub>4</sub>Ac extraction of soils) caesium-134 and 137.

22 The purpose of this paper is to describe the available data and methodology used for sample  
23 collection, sample preparation, and analysis. The data will be useful in the reconstruction of doses to  
24 human and wildlife populations, answering the current lack of scientific consensus on the effects of  
25 radiation on wildlife in the Chernobyl Exclusion zone and in evaluating future management options  
26 for Chernobyl impacted area of Ukraine and Belarus.

27 The data and supporting documentation are freely available from the Environmental Information Data  
28 Centre (EIDC) under the terms and conditions of the Open Government Licence (Kashparov et al.,  
29 2019 <https://doi.org/10.5285/a408ac9d-763e-4f4c-ba72-73bc2d1f596d>).

30  
31 **1 Background**

32 The dynamics of the releases of radioactive substance from the number four reactor at the  
33 Chernobyl nuclear power plant (ChNPP) and meteorological conditions over the ten days  
34 following the accident on the 26<sup>th</sup> April 1986 resulted in a complex pattern of contamination  
35 over most of Europe (IAEA, 2006).

36 The neutron flux rise and a sharp increase in energy emission at the time of the accident resulted  
37 in heating of the nuclear fuel and leakage of fission products. Destruction of the fuel rods  
38 caused an increase in heat transfer to the surface of the superheated fuel particles and coolant,  
39 and release of radioactive substances into the atmosphere (Kashparov et al., 1996). According  
40 to the latest estimates (Kashparov et al., 2003; UNSCEAR, 2008) 100% of inert radioactive  
41 gases (largely <sup>85</sup>Kr and <sup>133</sup>Xe), 20-60% of iodine isotopes, 12-40% of <sup>134,137</sup>Cs and 1.4-4% of  
42 less volatile radionuclides (<sup>95</sup>Zr, <sup>99</sup>Mo, <sup>89,90</sup>Sr, <sup>103,106</sup>Ru, <sup>141,144</sup>Ce, <sup>154,155</sup>Eu, <sup>238-241</sup>Pu etc.) in  
43 the reactor at the moment of the accident were released to the atmosphere.

44 As a result of the initial explosion on 26<sup>th</sup> April 1986, a narrow (100 km long and up to 1 km  
45 wide) relatively straight trace of radioactive fallout formed to the west of the reactor in the  
46 direction of Red Forest and Tolsty Les village (this has subsequently become known as the

47 ‘western trace’). This trace was mainly finely dispersed nuclear fuel (Kashparov et al., 2003,  
48 2018) and could only have been formed as a consequence of the short-term release of fuel  
49 particles with overheated vapour to a comparatively low height during night time (the accident  
50 occurred at 01:24) stable atmospheric conditions. At the time of the accident, surface winds  
51 were weak and did not have any particular direction; only at a height of 1500 m was there a  
52 south-western wind with the velocity  $8\text{--}10 \text{ m}\cdot\text{s}^{-1}$  (IAEA, 1992). Cooling of the release cloud,  
53 which included steam, resulted in the decrease of its volume, water condensation and wet  
54 deposition of radionuclides as mist (as the released steam cooled) (Saji, 2005). Later, the main  
55 mechanism of fuel particle formation was the oxidation of the nuclear fuel (Kashparov et al.,  
56 1996; Salbu et al., 1994). There was an absence of data on meteorological conditions in the  
57 area of ChNPP at the time of the accident (the closest observations were more than 100 km  
58 away to the west (Izrael et al., 1990)). There was also a lack of source term information and  
59 data on the composition of dispersed radioactive fallout. Consequently, it was not possible to  
60 make accurate predictions of deposition for the area close to the ChNPP (Talerko, 2005).

61 The relative leakage of fission products of uranium (IV) oxide in an inert environment at  
62 temperatures up to  $2600 \text{ }^{\circ}\text{C}$  decreases in the order: volatile (Xe, Kr, I, Cs, Te, Sb, Ag), semi-  
63 volatile (Mo, Ba, Rh, Pd, Tc) and nonvolatile (Sr, Y, Nb, Ru, La, Ce, Eu) (Kashparov et al.,  
64 1996; Pontillon et al., 2010). As a result of the estimated potential remaining heat release from  
65 fuel at the time of the accident ( $\sim 230 \text{ W kg}^{-1} \text{ U}$ ) and the heat accumulation in fuel (National  
66 Report of Ukraine, 2011), highly mobile volatile fission products (Kr, Xe, iodine, tellurium,  
67 caesium) were released from the fuel of the reactor and raised to a height of more than 1 km  
68 on 26<sup>th</sup> April 1986 and to approximately 600 m over the following days (IAEA, 1992; Izrael et  
69 al., 1990). The greatest release of radiocaesium occurred during the period of maximum heating  
70 of the reactor fuel on 26–28<sup>th</sup> April 1986 (Izrael et al., 1990). This caused the formation of the  
71 western, south-western (towards the settlements of Poliske and Bober), north-western  
72 (ultimately spreading to Sweden and wider areas of western Europe), and north-eastern  
73 condensed radioactive traces. Caesium deposition at distances from Chernobyl was largely  
74 determined by the degree of precipitation (e.g. see Chaplow et al. (2015) discussing deposition  
75 across Great Britain). After the covering of the reactor by dropping materials (including 40 t  
76 of boron carbide, 2500 t of lead, 1800 t of sand and clay, 800 t of dolomite) from helicopters  
77 over the period 27<sup>th</sup> April–10<sup>th</sup> May 1986 (National Report of Ukraine, 2011), the ability for  
78 heat exchange of the fuel reduced, which caused a rise of temperature and consequent increase  
79 of the leakage of volatile fission products and the melting of the materials which had been  
80 dropped onto the reactor. Subsequently, there was a sharp reduction in the releases of  
81 radionuclides from the destroyed reactor on 6<sup>th</sup> May 1986 (National Report of Ukraine, 2011)  
82 due to aluminosilicates forming thermally stable compounds with many fission products and  
83 fixing caesium and strontium at high temperature (a process known prior to the Chernobyl  
84 accident (Hilpert & Nurberg, 1983)).

85 The changes of the annealing temperature of the nuclear fuel during the accident had a strong  
86 effect on both the ratio of different volatile fission products released (the migratory properties  
87 of Xe, Kr, I, Te, Cs increased with the temperature rise and were influenced by the presence of  
88  $\text{UO}_2$ ) and the rate of destruction of the nuclear fuel which oxidised forming micronized fuel  
89 particles (Salbu et al., 1994; Kashparov et al., 1996). The deposition of radionuclides such as  
90  $^{90}\text{Sr}$ ,  $^{238\text{--}241}\text{Pu}$ ,  $^{241}\text{Am}$ , which were associated with the fuel component of the Chernobyl releases  
91 was largely limited to areas relatively close to the ChNPP. Areas receiving deposition of these

92 radionuclides were the Chernobyl Exclusion Zone (i.e. the area of approximately 30 km radius  
93 around the ChNPP), and adjacent territories in the north of the Kiev region, in the west of the  
94 Chernihiv region, and the Bragin and Hoyniki districts of the Gomel region (Belarus).  
95 Deposition was related to the rate of the dry gravitational sedimentation of the fuel particles  
96 caused by their high density (about 8-10 g·cm<sup>-3</sup> (Kashparov et al., 1996)); sedimentation of the  
97 lightweight condensation particles, containing iodine and caesium radioisotopes, was lower  
98 and hence these were transported further.

99 After the Chernobyl accident, western Europe and the Ukrainian-Belorussian Polessye were  
100 contaminated with radionuclides (IAEA, 1991, 1992, 2006). However, the area extending to  
101 60-km around the ChNPP was the most contaminated (Izrael et al., 1990). Work on the  
102 assessment of the radiological situation within the zone started within a few days of the  
103 accident; the aim of this work was the radiation protection of the population and personnel.  
104 Subsequently, further quantification of terrestrial dose rates was carried out by aerial-gamma  
105 survey by the State Hydrometeorological Committee together with Ministry of Geology and  
106 Ministry of Defence of USSR (as reported in Izrael et al., 1990). Large-scale sampling of soil  
107 was also conducted, with samples analysed using gamma-spectrometry and radiochemistry  
108 methods (see Izrael et al., 1990). These studies showed high variability in dose rates and  
109 radionuclide activity concentrations, with spatial patterns in both radioactive contamination  
110 and the radionuclide composition of fallout (Izrael et al., 1990).

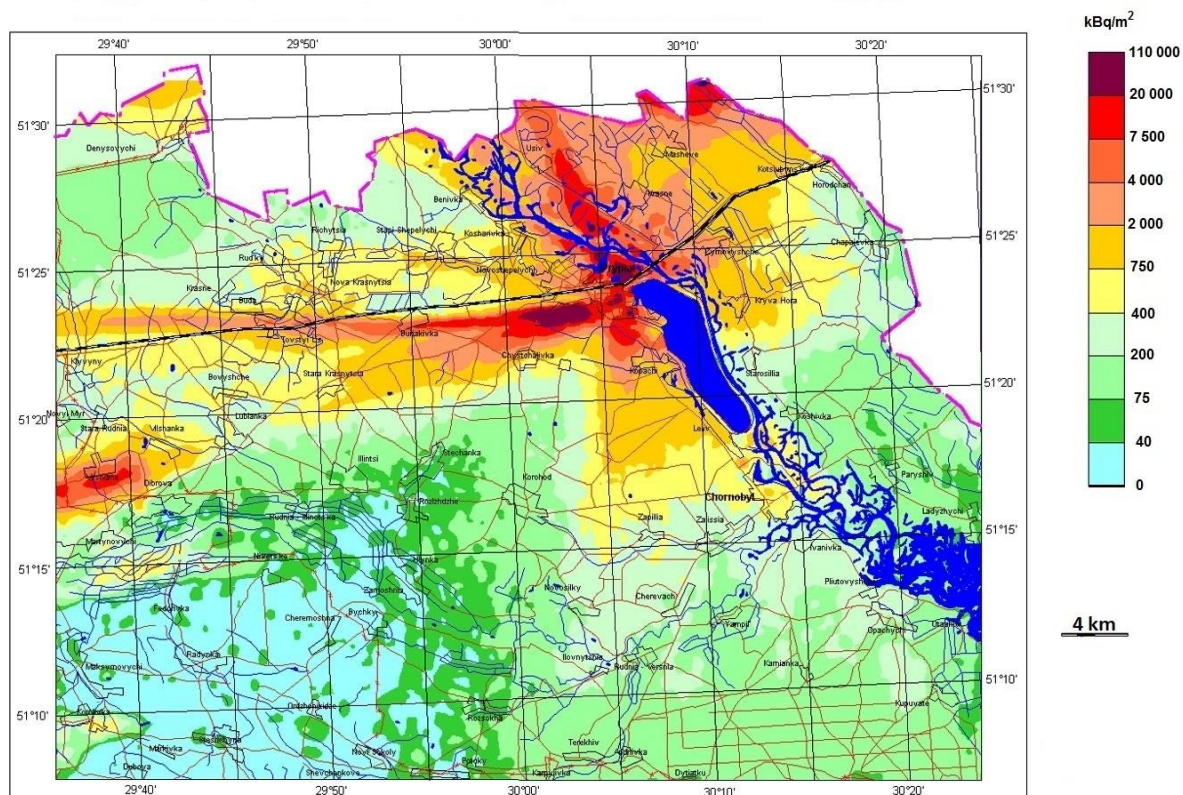
111 The initial area from which the population was evacuated was based on an arbitrary decision  
112 whereby a circle around the Chernobyl nuclear power plant with a radius of 30 km was defined  
113 (IAEA, 1991). In the initial phase after the accident (before 7<sup>th</sup> May 1986) 99195 people were  
114 evacuated from 113 settlements including 11358 people from 51 villages in Belarus and 87 837  
115 people from 62 settlements in Ukraine (including about 45 thousand people evacuated between  
116 14.00-17.00 hours on April 27 from the town of Pripyat located 4 km from the ChNPP)  
117 (Aleksakhin et al., 2001).

118 The analysis of data available in May 1986 showed that the extent of the territory with  
119 radioactive contamination where comprehensive measures were required to protect the  
120 population extended far beyond the 30 km Chernobyl Exclusion Zone (CEZ). A temporary  
121 annual effective dose limit of 100 mSv for the period from 26<sup>th</sup> April 1986 to 25<sup>th</sup> April 1987  
122 (50 mSv from external and 50 mSv from internal exposure) was set by the USSR Ministry of  
123 Health. To identify areas outside of the CEZ where the population required evacuation, dose  
124 criteria had to be defined. It was proposed to use the average value of the dose rate of gamma  
125 radiation in open air for an area (estimated for 10<sup>th</sup> May 1986) to help define an evacuation  
126 zone. An exposure dose rate of 5 mR h<sup>-1</sup> estimated for 10<sup>th</sup> May 1986 (approximating to an  
127 effective dose rate (EDR) of gamma radiation in air of 50  $\mu$ Sv h<sup>-1</sup>) equated to an external annual  
128 dose of 50 mSv for the period from 26<sup>th</sup> April 1986 to 25<sup>th</sup> April 1987.

129 At the end of May 1986 an approach to identify areas where evacuation was required using  
130 estimated internal dose rates was proposed. This used the average density of the surface  
131 contamination of the soil with long-lived biologically significant nuclides (<sup>137</sup>Cs, <sup>90</sup>Sr, <sup>239,240</sup>Pu)  
132 in a settlement and modelling to estimate the contamination of foodstuffs and hence diet. The  
133 numerical values suggested to identify areas for evacuation were: 15 Ci km<sup>-2</sup> (555 kBq m<sup>-2</sup>) of  
134 <sup>137</sup>Cs, 3 Ci km<sup>-2</sup> (111 kBq m<sup>-2</sup>) of <sup>90</sup>Sr and 0.1 Ci km<sup>-2</sup> (3.7 kBq m<sup>-2</sup>) of <sup>239,240</sup>Pu; this equated  
135 to an internal dose of 50 mSv over the first year after the accident.

136 However, in reality the main criterion for the evacuation was the exposure dose rate ( $R\ h^{-1}$ ) and  
137 where the exposure dose rate exceeded  $5\ mR\ h^{-1}$  (EDR in air of about  $50\ \mu\text{Sv}\ h^{-1}$ ) the evacuated  
138 population were not allowed to return.

139 Hence, in 1986 the boundary of the population evacuation zone was set at an exposure dose  
140 rate of  $5\ mR\ h^{-1}$  (EDR of about  $50\ \mu\text{Sv}\ h^{-1}$ ). However, the ratio of short-lived gamma-emitting  
141 radionuclides ( $^{95}\text{Zr}$ ,  $^{95}\text{Nb}$ ,  $^{106}\text{Ru}$ ,  $^{144}\text{Ce}$ ) deposited as fuel particles to  $^{134,137}\text{Cs}$  deposited as  
142 condensation particles, was inconsistent across the evacuated areas. Therefore, after the  
143 radioactive decay of the short-lived radionuclides the residual dose rate across the evacuated  
144 areas varied considerably and was largely determined by the pattern of long-lived  $^{137}\text{Cs}$   
145 deposition (e.g. Figure 1) (Kashparov et al., 2018).



146  
147 Figure 1. Caesium-137 deposition in the Ukrainian 30 km exclusion zone estimated for 1997  
148 (from UIAR, 1998).

149  
150 The first measurements of activity concentration of radionuclides in soil showed that  
151 radionuclide activity concentration ratios depended on distance and direction from the ChNPP  
152 (Izrael et al., 1990). Subsequent to this observation a detailed study of soil contamination was  
153 started in 1987 (Izrael et al., 1990). Taking into account the considerable heterogeneity of  
154 terrestrial contamination with radioactive substances in a large area, sampling along the  
155 western, southern and northern traces was carried out in stages finishing in 1988.

156 In 1987 the State Committee of Hydrometeorology of the USSR and the Scientific Centre of  
157 the Defence Ministry of the USSR established a survey programme to monitor radionuclide  
158 activity concentrations in soil. For this purpose, 540 sampling sites were identified at a distance  
159 of 5 km to 60 km around the ChNPP using a polar coordinate system centred on the ChNPP.  
160 Fifteen sampling sites were selected on each of the 36 rays drawn every 10 degrees (Loshchilov

161 et al., 1991) (Figures 3 and 4). Radionuclide activity concentrations in soil samples collected  
162 on the radial network were determined by the UIAR and used to calculate the radionuclide  
163 contamination density. These data are discussed in this paper and the full data set is freely  
164 available from Kashparov et al. (2019).

165

## 166 2 Data

167 The data (Kashparov et al., 2019) include location of sample sites (angle and distance from the  
168 ChNPP), dose rate, radionuclide deposition data, counting efficiency and information on  
169 exchangeable  $^{134,137}\text{Cs}$ .

170 The data are presented in a table with 21 columns and 540 rows of data (plus column headings)  
171 as one Microsoft Excel Comma Separated Value File (.csv) as per the requirements of the  
172 Environmental Information Data Centre. Appendix 1 presents an explanation of the column  
173 headings and units used in the data (Kashparov et al., 2019).

174

### 175 2.1 Sampling

176 To enable long-term monitoring and contamination mapping of the 60 km zone around the  
177 ChNPP, 540 points were defined and sampled in April – May 1987. The sampling strategy  
178 used a radial network with points at every 10° (from 10° to 360°); sampling points were located  
179 at distances of 5 km, 6 km, 7 km, 8.3 km, 10 km, 12 km, 14.7 km, 17 km, 20 km, 25 km, 30  
180 km, 37.5 km, 45 km, 52.5 km and 60 km (Figures 3 and 4). The locations of sampling points  
181 were identified using military maps (1:10000 scale) and local landscape. Sampling sites  
182 (identified using an index post) were estimated to be within 10 m of distances and directions  
183 as recorded in the accompanying data set. Sites were resampled regularly until 1990 and  
184 sporadically thereafter, however, data for these subsequent samplings are not reported here as  
185 they are unavailable (including to the UIAR).

186

187 Samples were not collected from points located in swamps, rivers and lakes; in total 489  
188 samples were collected. A corer with a diameter of 14 cm was used to collect soil samples  
189 down to a depth of 5 cm from five points at each location using the envelope method (with  
190 approximately 5-10 m between sampling points) (Figure 2) (Loshchilov et al., 1991). Soil cores  
191 were retained intact during transportation to the laboratory. At each sampling point, the  
192 exposure dose rate was determined 1 m above ground level.

193

194



195  
196

197 Figure 2. Soil sampling using a ring of 14 cm diameter to collect a 5 cm deep soil core (courtesy  
198 of UIAR, 1989).

199

## 200 2.2 Analysis

201 Using a high-purity germanium detector (GEM-30185, ORTEC, USA) and a multichannel  
202 analyser “ADCAM-300” (ORTEC, USA), the activity concentration of gamma emitting  
203 radionuclides (zirconium-95 ( $^{95}\text{Zr}$ ), niobium-95 ( $^{95}\text{Nb}$ ), ruthenium-106 ( $^{106}\text{Ru}$ ), caesium-134  
204 ( $^{134}\text{Cs}$ ), caesium-137, ( $^{137}\text{Cs}$ ) cerium-144 ( $^{144}\text{Ce}$ )) was determined in one soil sample from each  
205 sampling site. Information on gamma lines used in the analyses and radioisotope half-lives  
206 assumed for decay correction are presented in Appendix 2. Soil samples were analysed in a 1  
207 litre Marinelli container. The other four cores were sent to different laboratories in the Soviet  
208 Union (data for these cores are unfortunately not available). Using a 1M  $\text{NH}_4\text{Ac}$  solution (pH  
209 7) a 100 g subsample of soil was leached (solid: liquid ratio 1:5). The resultant leachate solution  
210 was shaken for 1 hour and then left at room temperature for 1 day before filtering through  
211 ashless filter paper (3-5  $\mu\text{m}$ ). The filtrate was then put into a suitable container for gamma  
212 analysis to determine the fraction of exchangeable  $^{134,137}\text{Cs}$ . Measured activity concentrations  
213 were reported at 68% confidence level (which equates to one standard deviation).

214 Decay radiation information from the master library, integrated in spectrum analysing software  
215 tool Gelicam (EG&G ORTEC, USA), was used in gamma-analyses. Activities of  $^{106}\text{Ru}$  and  
216  $^{137}\text{Cs}$  in samples were estimated via their gamma radiation emitting progenies  $^{106}\text{Rh}$  and  $^{137\text{m}}\text{Ba}$ ,  
217 respectively.

218

219 Calibration of the spectrometer was conducted using certified standards (soil equivalent multi-  
220 radionuclide standard, V. G. Khlopin Radium Institute, Russia). Quality assurance/quality  
221 control procedures included regular monitoring of the system performance, efficiency,  
222 background and full width at half maximum (FWHM) for the  $^{144}\text{Ce}$ ,  $^{137}\text{Cs}$  and  $^{95}\text{Nb}$  photo  
223 peaks. To validate accuracy and precision of the method employed for  $^{137}\text{Cs}$  activity  
224 concentration measurements, quality control samples (i.e., different matrix samples including  
225 water, soil and sawdust spiked with known certified activities of radionuclides) and Certified  
226 Reference Materials (CRM) were analysed alongside the samples. Analysis of IAEA CRMs  
227 showed satisfactory results for radionuclide mean activity concentrations with results being  
228 within the 95% confidence interval; the limit of detection for  $^{137}\text{Cs}$  in all samples was 1 Bq.

229 Subsamples were analysed in a different laboratory (USSR Ministry of Defence) and results  
230 for the two laboratories were within the error of determination.

231  
232 The density of soil contamination ( $\text{Bq m}^{-2}$ ) was calculated from the estimated radionuclide  
233 activity concentrations in soils. It has been estimated that uncertainty from using a single soil  
234 sample (of area  $0.015 \text{ m}^2$ ) to estimate the value of contamination density of a sampling site (i.e.  
235 the area from which five cores were collected) may be up to 50% (IAEA, 2019).

236  
237 The data described in this paper (Kashparov et al., 2020) comprise exposure dose rate ( $\text{mR/h}$ ),  
238 date of gamma activity measurement, density of contamination ( $\text{Bq m}^{-2}$ ) of  $^{95}\text{Zr}$ ,  $^{95}\text{Nb}$ ,  $^{106}\text{Ru}$ ,  
239  $^{134}\text{Cs}$ ,  $^{137}\text{Cs}$  and  $^{144}\text{Ce}$  (with associated activity measurement uncertainties) and density of  
240 contamination of  $^{134+137}\text{Cs}$  in exchangeable form. Reported radionuclide activity concentration  
241 values are for the date of measurement (samples were analysed within 1.5 months of  
242 collection).

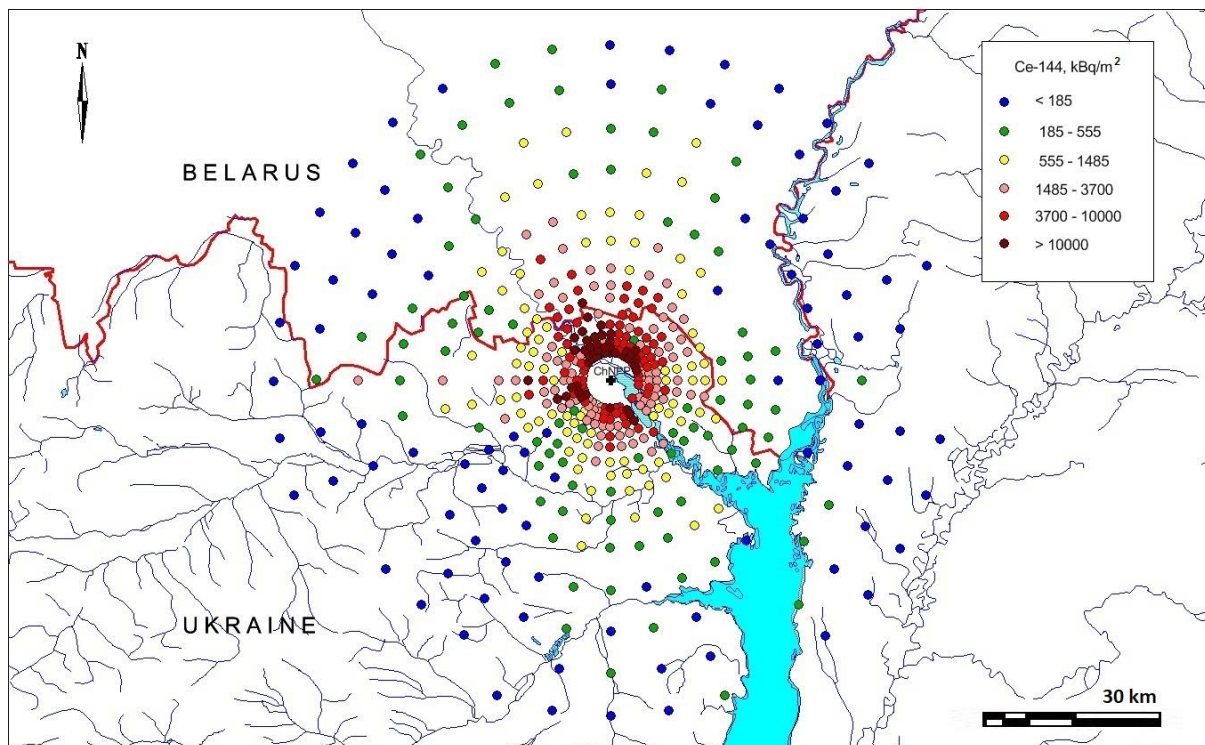
243  
244 For presentation below, radionuclide activity concentrations have been decay corrected to 6th  
245 May 1986 (the date on which releases from the reactor in-effect stopped) using the equation:  
246  $A_T = A_0 / e^{-\lambda t}$  where  $A_T$  equals the radionuclide activity concentration at the time of measurement  
247 ( $t$ );  $A_0$  is the activity concentration on 6<sup>th</sup> May 1986, and  $\lambda$  is the decay constant (i.e.  
248 0.693/radionuclide physical half-life (see Table 1 for radionuclide half-lives)).

## 249 2.3 Results

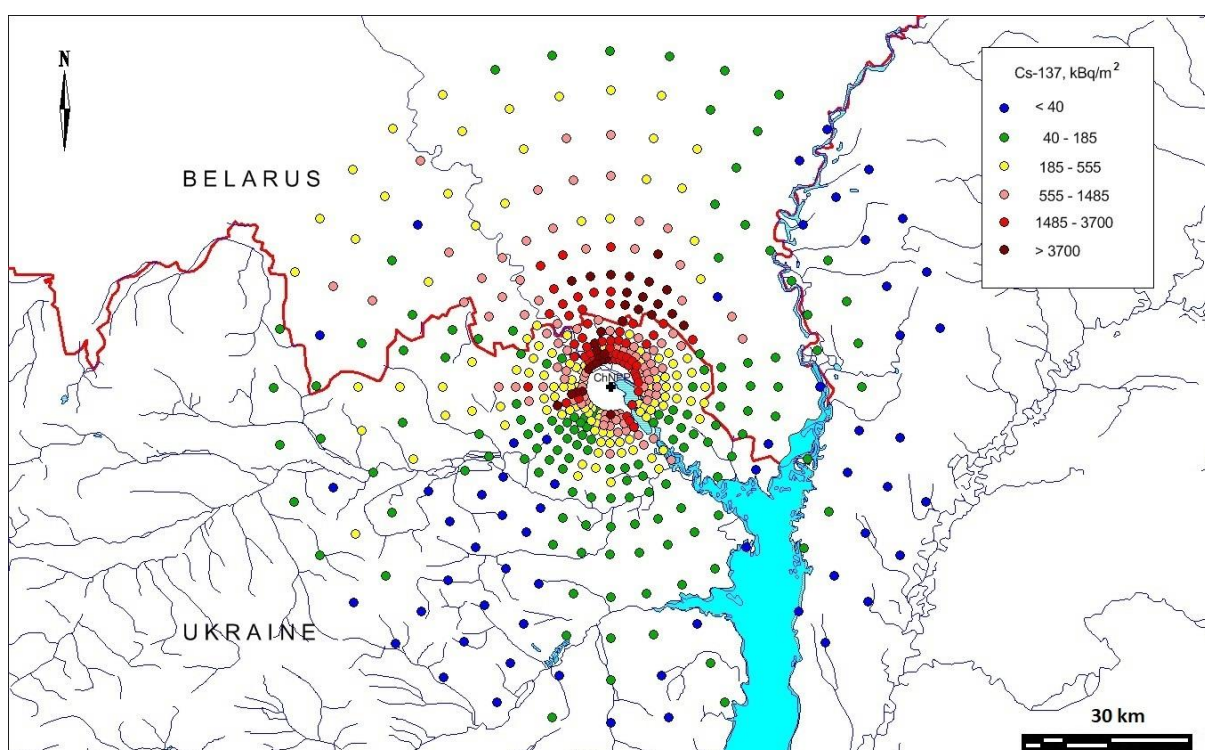
250  
251 The contamination density of  $^{144}\text{Ce}$  and  $^{137}\text{Cs}$  are presented in Figure 3 and 4; the activity  
252 concentrations as presented in the figures have been decay corrected to 6th May 1986. The  
253 density of  $^{144}\text{Ce}$  contamination decreased exponentially with distance (Figures 3 and 5),  
254 because  $^{144}\text{Ce}$  was released in the fuel particles, which had a high dry deposition velocity  
255 (Kuriny et al., 1993). The fallout density of  $^{144}\text{Ce}$  decreased by 7-9 times between the 5 km and  
256 30 km sampling sites, and by 70-120 times between the 5 km and 60 km sampling sites (Figure  
257 5).

258  
259 The fallout density of  $^{137}\text{Cs}$  decreased similarly to that of  $^{144}\text{Ce}$  along the southern ‘fuel trace’  
260 (Figure 5a). The contamination density of  $^{137}\text{Cs}$  along the western trace decreased less than the  
261  $^{144}\text{Ce}$  contamination density due to the importance of the condensation component of the fallout  
262 in this direction (with a resultant  $R^2$  value for the relationship between  $^{137}\text{Cs}$  and distance lower  
263 than seen for  $^{144}\text{Ce}$  and  $^{137}\text{Cs}$  in different directions) (Figure 5b). The comparative decrease of  
264  $^{137}\text{Cs}$  contamination density along the northern trace (mixed fuel and condensation fallout) was  
265 in between that of the southern and western traces (Figure 5c) although there were caesium  
266 hotspots in the northern condensation trace (Figures 4 and 5c). The activity ratio of  $^{144}\text{Ce}$  to  
267  $^{137}\text{Cs}$  decreased with distance from the ChNPP due to the condensation component being more  
268 important for  $^{137}\text{Cs}$ ; the condensation component had a lower deposition velocity compared  
269 with fuel particles (with which  $^{144}\text{Ce}$  was associated) (Figure 6). The ratio  $^{144}\text{Ce}/^{137}\text{Cs}$  for  
270 Chernobyl reactor fuel on 6<sup>th</sup> May 1986 can be estimated to be 15 from data presented in Table  
271 1. The ratio was about 11 (geometric mean of 1167 measurements) in Chernobyl fuel particles  
272 larger than  $10 \mu\text{m}$  due to caesium escape during high-temperature annealing (Kuriny et al.,  
273 1993). The ratio of  $^{144}\text{Ce}/^{137}\text{Cs}$  in deposition exceeded five in the south-east and in the south  
274 up to 60 km and 30 km from the NPP respectively (Figure 6). Thus, activities of  $^{134,137}\text{Cs}$  in the  
275 condensate and in the fuel components in these directions were of approximate equal  
276 importance. The condensation component of caesium was more important in the north and

277 dominated in the west (Figure 8) (Loshchilov et al., 1991; Kuriny et al., 1993); the more rapidly  
278 changing  $^{144}\text{Ce}/^{137}\text{Cs}$  ratios in these directions are reflective of this (Figure 6).

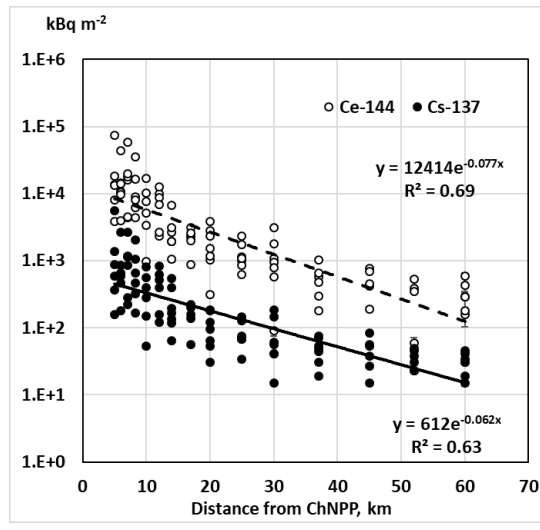


279  
280 Figure 3. The fallout density of  $^{144}\text{Ce}$  (kBq/m<sup>2</sup>) within the 60 km zone around the ChNPP  
281 decay corrected to 6<sup>th</sup> May 1986.



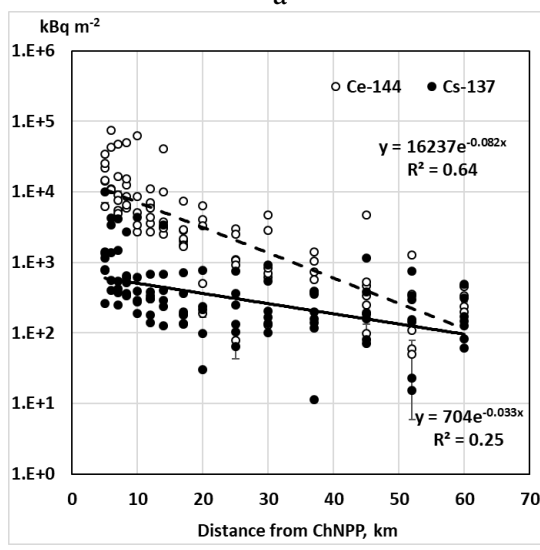
283  
284 Figure 4. The fallout density of  $^{137}\text{Cs}$  (kBq/m<sup>2</sup>) within the 60 km zone around the ChNPP  
285 decay corrected to 6<sup>th</sup> May 1986.

286  
287



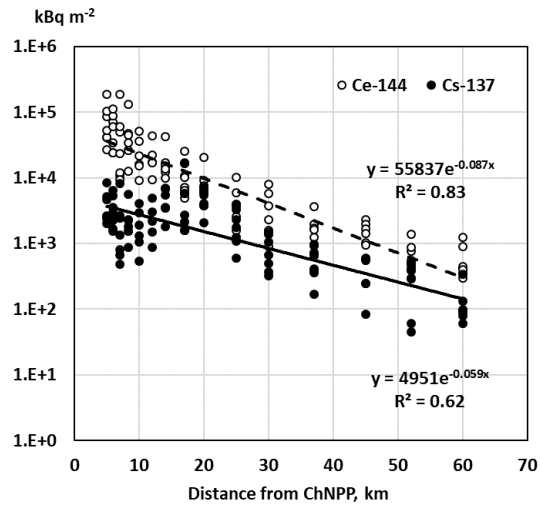
a

288  
289



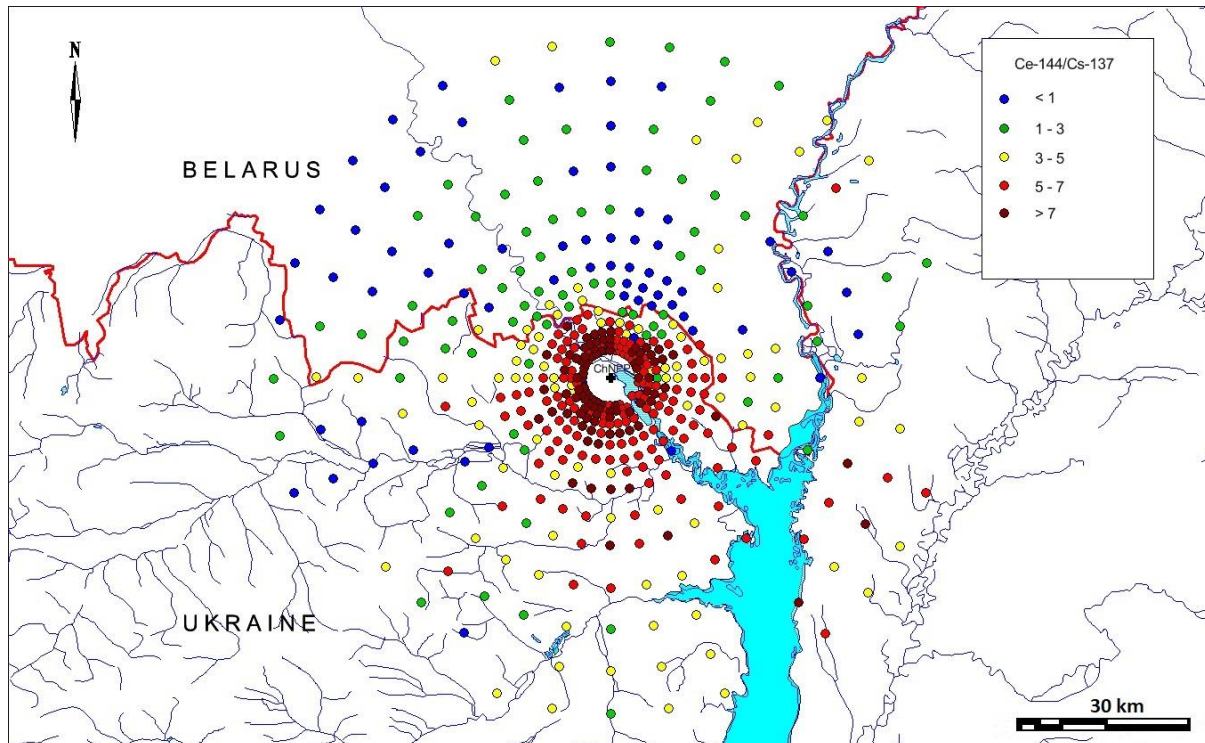
b

290  
291



c

292  
293 Figure 5. Relationship between fallout density of  $^{144}\text{Ce}$  (1) and  $^{137}\text{Cs}$  (2) and distance from the ChNPP towards the south (a) (150-210°), the west (b) (240-300°) and the north (c) (330-30°).



298 Figure 6.  $^{144}\text{Ce}/^{137}\text{Cs}$  ratio within the 60 km zone around the ChNPP decay corrected to 6<sup>th</sup>  
 299 May 1986.

301 Table 1. The average activity concentrations of radionuclides with half-life ( $T_{1/2}$ )  $>1$  day  
 302 estimated in the fuel of the ChNPP number four reactor recalculated for 6<sup>th</sup> May 1986  
 303 (Begichev et al., 1993).

Radionuclide	Half-life (days)	Average activity concentration ( $\text{Bq g}^{-1}$ )	Radionuclide	Half-life (days)	Average activity concentration ( $\text{Bq g}^{-1}$ )
$^{75}\text{Se}$	$1.2 \times 10^2$	$5.4 \times 10^6$	$^{132}\text{Te}$	$3.3 \times 10^0$	$2.4 \times 10^{10}$
$^{76}\text{As}$	$1.1 \times 10^0$	$1.7 \times 10^7$	$^{133}\text{Xe}$	$5.2 \times 10^0$	$3.4 \times 10^{10}$
$^{77}\text{As}$	$1.6 \times 10^0$	$4.1 \times 10^7$	$^{134}\text{Cs}$	$7.6 \times 10^2$	$8.9 \times 10^8$
$^{82}\text{Br}$	$1.5 \times 10^0$	$1.8 \times 10^9$	$^{135}\text{Cs}$	$5.5 \times 10^7$	$1.9 \times 10^4$
$^{85}\text{Kr}$	$3.9 \times 10^3$	$1.5 \times 10^8$	$^{136}\text{Cs}$	$1.3 \times 10^1$	$3.3 \times 10^{10}$
$^{86}\text{Rb}$	$1.9 \times 10^1$	$8.7 \times 10^9$	$^{137}\text{Cs}$	$1.1 \times 10^4$	$1.4 \times 10^9$
$^{89}\text{Sr}$	$5.1 \times 10^1$	$2.1 \times 10^{10}$	$^{140}\text{Ba}$	$1.3 \times 10^1$	$3.2 \times 10^{10}$
$^{90}\text{Sr}$	$1.1 \times 10^4$	$1.2 \times 10^9$	$^{141}\text{Ce}$	$3.3 \times 10^1$	$2.9 \times 10^{10}$
$^{90}\text{Y}$	$1.1 \times 10^4$	$1.2 \times 10^9$	$^{143}\text{Ce}$	$1.4 \times 10^0$	$2.9 \times 10^{10}$
$^{91}\text{Y}$	$5.9 \times 10^1$	$2.6 \times 10^{10}$	$^{144}\text{Ce}$	$2.8 \times 10^2$	$2.1 \times 10^{10}$
$^{95}\text{Zr}$	$6.4 \times 10^1$	$3.1 \times 10^{10}$	$^{147}\text{Nd}$	$1.1 \times 10^1$	$1.1 \times 10^{10}$
$^{95}\text{Nb}$	$3.5 \times 10^1$	$3.0 \times 10^{10}$	$^{147}\text{Pm}$	$9.5 \times 10^2$	$4.2 \times 10^9$

<sup>96</sup> Nb	$9.8 \times 10^1$	$3.1 \times 10^{10}$	<sup>148m</sup> Pm	$4.1 \times 10^1$	$8.5 \times 10^9$
<sup>99</sup> Mo	$2.7 \times 10^0$	$3.2 \times 10^{10}$	<sup>149</sup> Nd	$2.2 \times 10^0$	$5.8 \times 10^9$
<sup>99m</sup> Tc	$2.7 \times 10^0$	$2.8 \times 10^{10}$	<sup>151</sup> Pm	$1.2 \times 10^0$	$2.6 \times 10^9$
<sup>103</sup> Ru	$3.9 \times 10^1$	$2.0 \times 10^{10}$	<sup>151</sup> Sm	$3.3 \times 10^4$	$3.4 \times 10^7$
<sup>105</sup> Rh	$1.5 \times 10^0$	$1.0 \times 10^{10}$	<sup>153</sup> Sm	$1.9 \times 10^0$	$1.1 \times 10^9$
<sup>106</sup> Ru	$3.7 \times 10^2$	$4.5 \times 10^9$	<sup>154</sup> Eu	$3.1 \times 10^3$	$3.7 \times 10^7$
<sup>110m</sup> Ag	$2.5 \times 10^2$	$5.3 \times 10^8$	<sup>155</sup> Eu	$1.7 \times 10^3$	$4.85 \times 10^7$
<sup>111</sup> Ag	$7.5 \times 10^0$	$4.4 \times 10^8$	<sup>156</sup> Eu	$1.5 \times 10^1$	$1.9 \times 10^8$
<sup>115m</sup> In	$1.9 \times 10^1$	$8.6 \times 10^7$	<sup>160</sup> Tb	$7.2 \times 10^1$	$1.0 \times 10^7$
<sup>117m</sup> Sn	$1.4 \times 10^1$	$8.3 \times 10^7$	<sup>237</sup> Np	$7.8 \times 10^8$	$1.4 \times 10^3$
<sup>123</sup> Sn	$1.3 \times 10^2$	$9.9 \times 10^7$	<sup>239</sup> Np	$2.4 \times 10^0$	$3.1 \times 10^{11}$
<sup>124</sup> I	$4.2 \times 10^0$	$1.4 \times 10^8$	<sup>236</sup> Pu	$1.0 \times 10^3$	$6.0 \times 10^2$
<sup>125</sup> Sb	$1.0 \times 10^3$	$7.8 \times 10^7$	<sup>238</sup> Pu	$3.2 \times 10^4$	$6.8 \times 10^6$
<sup>125m</sup> Te	$5.8 \times 10^1$	$1.6 \times 10^7$	<sup>239</sup> Pu	$8.8 \times 10^6$	$5.0 \times 10^6$
<sup>126m</sup> Sb	$1.2 \times 10^1$	$4.4 \times 10^8$	<sup>240</sup> Pu	$2.4 \times 10^6$	$7.8 \times 10^6$
<sup>126</sup> Sb	$1.2 \times 10^1$	$6.1 \times 10^7$	<sup>241</sup> Pu	$5.1 \times 10^3$	$9.6 \times 10^8$
<sup>127</sup> Sb	$3.8 \times 10^0$	$1.1 \times 10^9$	<sup>242</sup> Pu	$1.4 \times 10^8$	$1.5 \times 10^4$
<sup>127</sup> Te	$1.1 \times 10^2$	$8.9 \times 10^8$	<sup>241</sup> Am	$1.6 \times 10^5$	$8.7 \times 10^5$
<sup>129m</sup> Te	$3.3 \times 10^1$	$5.5 \times 10^9$	<sup>243</sup> Am	$2.7 \times 10^6$	$5.1 \times 10^4$
<sup>131</sup> I	$8.0 \times 10^0$	$1.6 \times 10^{10}$	<sup>242</sup> Cm	$1.6 \times 10^2$	$2.3 \times 10^8$
<sup>131m</sup> Xe	$1.2 \times 10^1$	$1.8 \times 10^8$	<sup>244</sup> Cm	$6.6 \times 10^3$	$2.2 \times 10^6$

305

306 A good correlation ( $R^2=0.98$ ) was observed between fallout densities of <sup>95</sup>Zr (estimated from  
 307 the activity concentration of daughter product <sup>95</sup>Nb)<sup>1</sup> and <sup>144</sup>Ce (Figure 7a) because both  
 308 radionuclides were released and deposited as fuel particles (Kuriny et al., 1993; Kashparov et  
 309 al., 2003; Kashparov, 2003). The fallout density ratio of <sup>144</sup>Ce/<sup>95</sup>Zr=0.73±0.05, decay corrected  
 310 to 6th May 1986 was similar to that estimated for Chernobyl reactor fuel (<sup>144</sup>Ce/<sup>95</sup>Zr=0.68)  
 311 (Table 1).

312 The activity ratio of <sup>144</sup>Ce to <sup>106</sup>Ru in fallout was correlated ( $R^2=0.93$ ) and was 3.9±0.4 decay  
 313 corrected to 6<sup>th</sup> May 1986 (Figure 7b). The value was close to the ratio of <sup>144</sup>Ce/<sup>106</sup>Ru estimated  
 314 for fuel in the ChNPP number four reactor (4.7) (Table 1). Excess <sup>106</sup>Ru activity relative to  
 315 <sup>144</sup>Ce activity in some soil samples was observed likely due to the presence of “ruthenium  
 316 particles” (a matrix of iron group elements with a high content of <sup>103,106</sup>Ru (Kuriny et al., 1993;  
 317 Kashparov et al., 1996)).

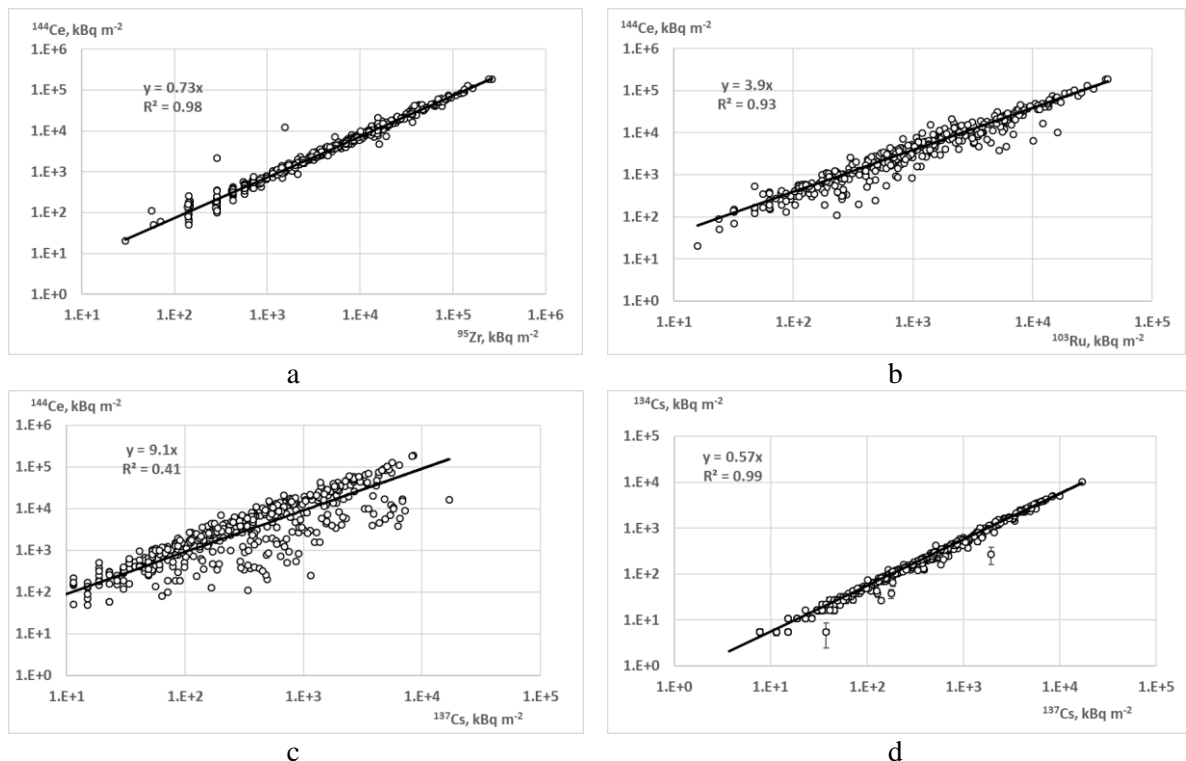
318 There was a weak correlation ( $R^2=0.41$ ) between <sup>144</sup>Ce and <sup>137</sup>Cs activities in the fallout  
 319 because, as already discussed, caesium was largely deposited as condensation particles while  
 320 cerium was deposited in fuel particles only. However, in highly contaminated areas close to  
 321 the ChNPP a significant part of the <sup>137</sup>Cs was deposited as fuel particles and the activity ratio  
 322 of <sup>144</sup>Ce/<sup>137</sup>Cs of 9.1 (Figure 7c) broadly corresponded to that of 15 in the reactor fuel (Table  
 323 1).

<sup>1</sup> Niobium-95 ( $T_{1/2}=34$  days) is the daughter radionuclide of <sup>95</sup>Zr ( $T_{1/2}=65$  days) and the ratio of their activities at an equilibrium equals <sup>95</sup>Nb/<sup>95</sup>Zr=2.1.

324

325 Different radioisotopes of caesium escaped from nuclear fuel and were deposited in the same  
 326 way. This similar behaviour of  $^{134}\text{Cs}$  and  $^{137}\text{Cs}$  resulted in a strong correlation ( $R^2=0.99$ )  
 327 between their activities in soil samples and the ratio of  $^{134}\text{Cs}/^{137}\text{Cs}=0.57\pm0.07$  was similar to  
 328 that estimated for the reactor fuel (0.64, Table 1).

329



330 Figure 7. Correlation between deposition densities of different radionuclides decay corrected  
 331 to 6<sup>th</sup> May 1986.

332

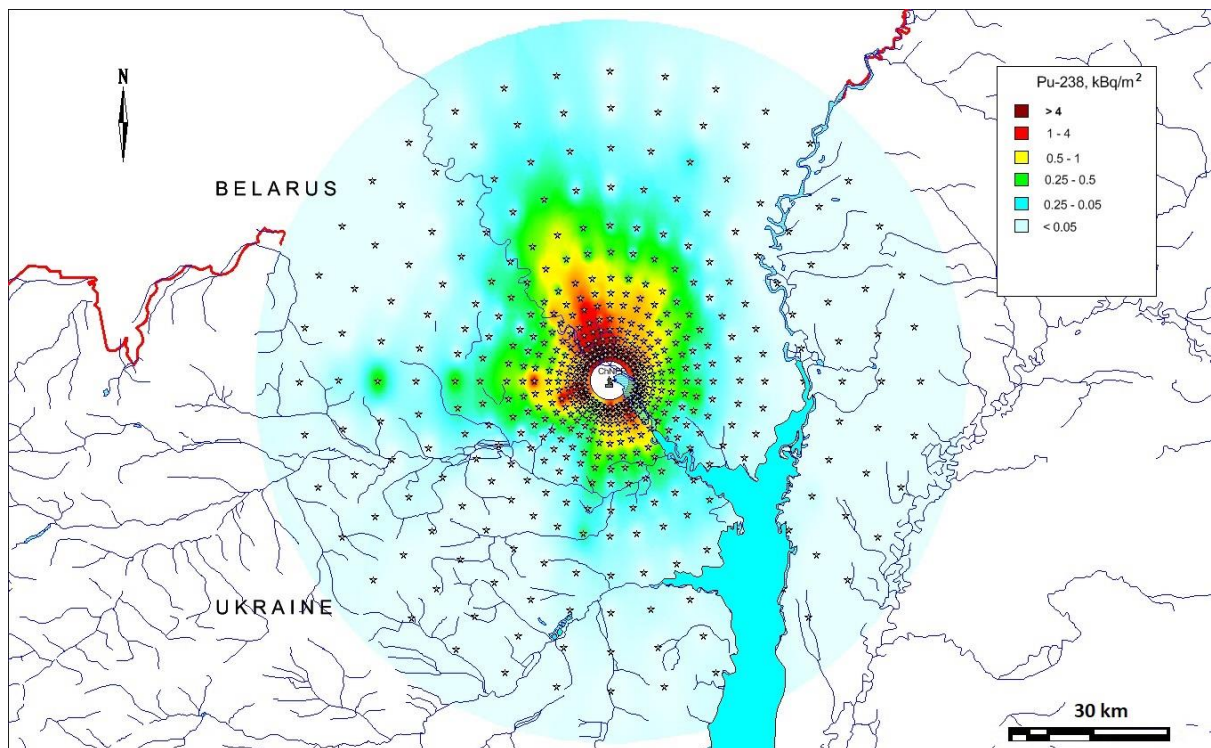
### 333 3 Use of the data

334 Apart from adding to the available data with which contamination maps for the CEZ and  
 335 surrounding areas can be generated (e.g. Kashparov et al., 2018) the data discussed in this paper  
 336 can be used to make predictions for less well studied radionuclides.

337 The determination of beta and alpha emitting radionuclides in samples requires radiochemical  
 338 extraction which is both time consuming and relatively expensive. Large-scale surveys of the  
 339 deposition of alpha and beta emitting radionuclides are therefore more difficult than those for  
 340 gamma-emitting radionuclides and are not conducive with responding to a large-scale accident  
 341 such as that which occurred at Chernobyl. Above we have demonstrated that the deposition  
 342 behaviour of different groups of radionuclides was determined by the form in which they were  
 343 present in the atmosphere (i.e. associated with fuel particles or condensation particles).

344 We propose that  $^{144}\text{Ce}$  deposition can be used as a marker of the deposition of fuel particles;  
 345 fuel particles were the main deposition form of nonvolatile radionuclides (i.e. Sr, Y, Nb, Ru,  
 346 La, Ce, Eu, Np, Pu, Am, Cm). Therefore, using  $^{144}\text{Ce}$  activity concentrations determined in soil  
 347 samples and estimates of the activities in reactor fuel, we can make estimates of the deposition

348 of radionuclides such as Pu-isotopes and Cm that have been relatively less studied. For  
 349 example, activity ratios of  $^{238}\text{Pu}$ ,  $^{239}\text{Pu}$   $^{240}\text{Pu}$  and  $^{241}\text{Pu}$  to  $^{144}\text{Ce}$ , at the time of measurement  
 350 would be  $8.4 \times 10^{-4}$ ,  $6.2 \times 10^{-4}$ ,  $9.7 \times 10^{-4}$  and  $1.1 \times 10^{-1}$  respectively (estimated by decay correcting  
 351 data presented in Table 1). Fallout densities of these plutonium isotopes can therefore be  
 352 calculated for all sampling points where deposition density of  $^{144}\text{Ce}$  was measured either in this  
 353 study (e.g. Figure 3) or in other data sets. As an example of the application of the data in this  
 354 manner, Figure 8 presents the estimated deposition of  $^{238}\text{Pu}$ ; Figure 8 was prepared using the  
 355 TIN (triangulated irregular network) interpolation within MAPINFO. The first maps of  $^{90}\text{Sr}$   
 356 and  $^{239+240}\text{Pu}$  surface contamination from the Chernobyl accident were prepared in the frame  
 357 of an international project (IAEA, 1992) in a similar way.



358 Figure 8. The fallout density of  $^{238}\text{Pu}$  ( $\text{kBq m}^{-2}$ ) corrected to 6<sup>th</sup> May 1986; estimated from  
 359 measurements of  $^{144}\text{Ce}$  in soil and estimated activity concentrations in the fuel of the ChNPP  
 360 reactor number four (note no data were available for less than 5 km from ChNPP and no  
 361 interpolation for this area has been attempted).

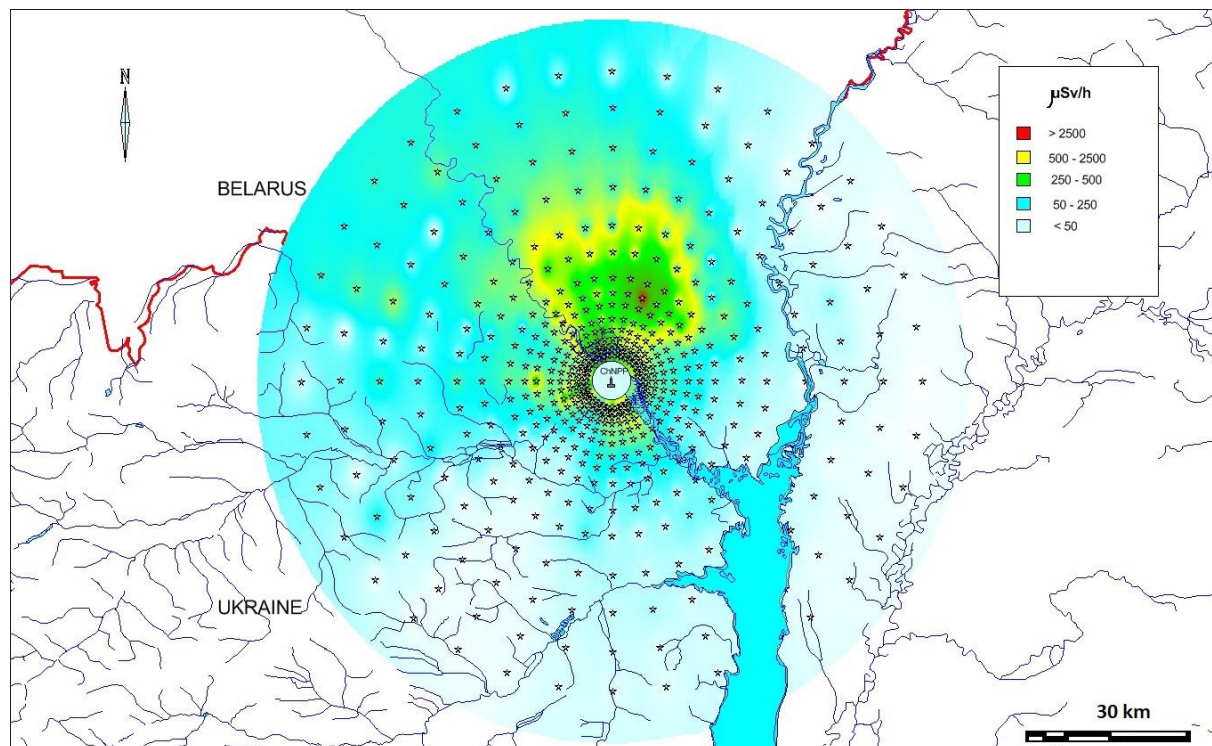
363 The dynamic spatial distribution of gamma dose rate can be reconstructed using the data on  
 364 radionuclide contamination densities (Kashparov et al., 2019) in combination with the ratios  
 365 between activities of radionuclides in fuel and in condensed components of Chernobyl fallout  
 366 (Table 1) and also dose coefficients for exposure to contaminated ground surfaces, ( $\text{Sv s}^{-1}/\text{Bq}$   
 367  $\text{m}^{-2}$ ) (Eckerman & Ryman, 1993). Five days after deposition the following radionuclides were  
 368 major contributors (about 95 %) to gamma dose rate:  $^{136}\text{Cs}$ ,  $^{140}\text{La}$ ,  $^{239}\text{Np}$ ,  $^{95}\text{Nb}$ ,  $^{95}\text{Zr}$ ,  $^{131}\text{I}$ ,  $^{148m}\text{Pm}$ ,  
 369  $^{103}\text{Ru}$ ,  $^{140}\text{Ba}$ ,  $^{132}\text{Te}$ . After three months the major external dose contributors were:  $^{95}\text{Nb}$ ,  
 370  $^{95}\text{Zr}$ ,  $^{148m}\text{Pm}$ ,  $^{134}\text{Cs}$ ,  $^{103}\text{Ru}$ ,  $^{137m}\text{Ba}$ ,  $^{110m}\text{Ag}$ ,  $^{136}\text{Cs}$ ,  $^{106}\text{Rh}$ . Three years after the major contributors  
 371 were  $^{137m}\text{Ba}$ ,  $^{134}\text{Cs}$ ,  $^{106}\text{Rh}$ ,  $^{110m}\text{Ag}$ ,  $^{154}\text{Eu}$ . At the present time the gamma dose can be estimated  
 372 to be mainly (99%) due to the gamma-emitting daughter radionuclide of  $^{137}\text{Cs}$  ( $^{137m}\text{Ba}$ ). Bondar  
 373 (2015) from a survey of the CEZ along the Ukrainian-Belarussian border, showed a good  
 374 relationship between  $^{137}\text{Cs}$  contamination ( $A_{\text{Cs-137}}$ , in the range of 17-7790  $\text{kBq m}^{-2}$ ) and

375 ambient dose rates at 1m above the ground ( $D_{ext}$ , in the range of 0.1-6.0  $\mu\text{Sv h}^{-1}$ ). The  
376 relationship was described by following equation with correlation coefficient of 0.99:

377 
$$D_{ext} = 0.0009 \cdot A_{Cs-137} + 0.14.$$

378 As an example of the application of the data in this manner, Figure 9 presents the estimated  
379 external effective gamma dose rate five and 95 days after the cessation of the radioactive  
380 releases from the reactor on 6<sup>th</sup> May 1986.

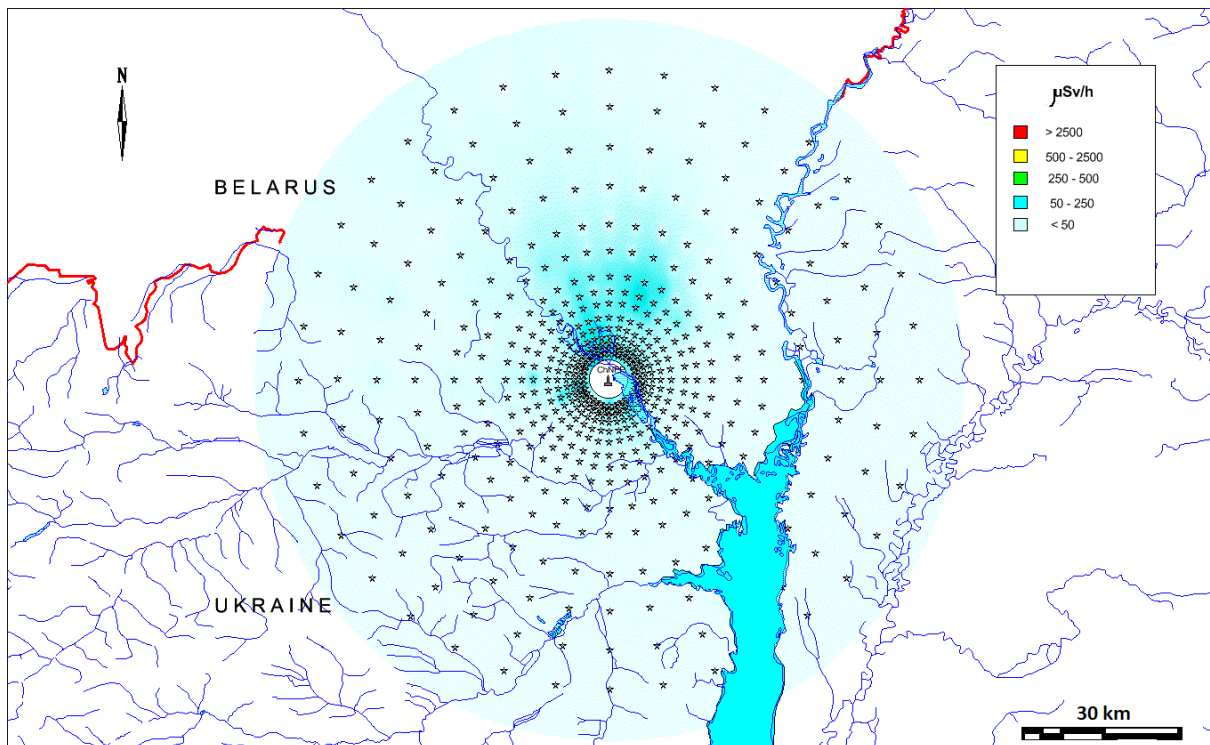
381



382

383

a



384

385

b

386 Figure 9. Spatial distribution, interpolated as for Figure 8, of effective dose rate within the 60  
 387 km zone around the ChNPP on 10<sup>th</sup> May 1986 (a) and 10<sup>th</sup> August 1986 (b). Note no data  
 388 were available for less than 5 km from ChNPP and no interpolation for this area has been  
 389 attempted.

390

391 The estimated effective dose rate values exceed the evacuation dose criteria of 50  $\mu\text{Sv h}^{-1}$  over  
 392 a large area (especially in the north and west) of the 60 km area around the ChNPP on 10<sup>th</sup> May  
 393 1986 (Figure 9a); as discussed above a dose rate of 50  $\mu\text{Sv h}^{-1}$  on 10<sup>th</sup> May 1986 equated to a  
 394 total dose over the first year after the accident of 50 mSv - the value used to define areas for  
 395 evacuation. On the 10<sup>th</sup> August 1986 the area estimated to exceed 50  $\mu\text{Sv h}^{-1}$  was restricted to  
 396 the north (Figure 9b). The dose rate decreased quickly after the accident due to the radioactive  
 397 decay of short-lived radionuclides. The dominance of these short-lived radionuclides and a lack  
 398 of knowledge of the radionuclide composition of the fallout made it difficult in 1986 to estimate  
 399 external dose rates to the public for an evaluation date of 10<sup>th</sup> May 1986 (most dose rate  
 400 measurements being made after the 10<sup>th</sup> May). This likely resulted in the overestimation of  
 401 dose rates for some villages in 1986 leading to their evacuation when the external dose rate  
 402 would not have been in excess of the 50 mSv limit used by the authorities.

403 There is a need for deposition data for the CEZ and surrounding areas for a number of reasons.  
 404 These include exploring risks associated with future management options for the CEZ (e.g.  
 405 management of the water table, forest fire prevention, increased tourism, etc.) and also the  
 406 return of abandoned areas outside of the CEZ to productive use. The long-term effect of  
 407 radiation exposure on wildlife in the CEZ is an issue of much debate (e.g. see discussion in  
 408 Beresford et al., 2019). Improved data which can be used to map the contamination of a range  
 409 of radionuclides will be useful in improving dose assessments to wildlife (including  
 410 retrospective assessments of earlier exposure rates). The CEZ has been declared a

411 'Radioecological Observatory' (Muikku et al., 2018) (where a Radioecology Observatory is  
412 defined as a radioactively contaminated field site that provides a focus for joint, long-term,  
413 radioecological research). The open provision of data as described in this paper fosters the spirit  
414 of collaboration and openness required to make the observatory site concept successful and  
415 joins a growing amount of data made available for the CEZ (Kashparov et al., 2017; Fuller et  
416 al., 2018; Kendrick et al., 2018; Gaschak et al., 2018; Beresford et al., 2018; Lerebours and  
417 Smith, 2019).

#### 418 **4 Data availability**

419 The data described here have a digital object identifier (doi: 10.5285/a408ac9d-763e-4f4c-  
420 ba72-73bc2d1f596d) and are freely available for registered users from the NERC  
421 Environmental Information Data Centre (<http://eidc.ceh.ac.uk/>) under the terms of the Open  
422 Government Licence (Kashparov et al., 2019).

423 Competing interests. The authors declare that they have no conflict of interest.

424 Acknowledgements. Funding for UKCEH staff to contribute to preparing this paper and the  
425 accompanying data set (Kashparov et al., 2019) was provided by the TREE project  
426 (<http://www.ceh.ac.uk/tree>; funded by NERC, the Environment Agency and Radioactive  
427 Waste Management Ltd under the RATE programme) and associated iCLEAR  
428 (<https://tree.ceh.ac.uk/content/iclear-0>; funded by NERC) projects.

429 Author contribution. Soil samples were collected by the USSR Ministry of Defence and  
430 delivered to UIAR. Sample preparation, analysis and data interpretation was carried out by  
431 UIAR staff contributing as follows: Kashparov, Levchuk, Protsak, - sample preparation,  
432 measurement of radionuclide activity concentrations in samples; Kashparov - analysis of  
433 results; Zhurba - database creation and preparation of the manuscript figures (maps). The  
434 manuscript was prepared by Chaplow, Beresford, Kashparov, Levchuk and Zhurba.  
435

#### 436 **References**

437 Aleksakhin, R.M., Buldakov, L.A., Gubanov, V.A., Drozhko, E.G., Ilyin, L.A., Kryshev, I.I., Linge, I.I., Romanov, G.N.,  
438 Savkin, M.N., Saurov, M.M., Tikhomirov, F.A., Kholina, Yu.B. Major radiation accidents: consequences and protective  
439 measures. Edited by L.A. Ilyin and V.A. Gubina. book published in Moscow, Publishing House IzdAT. 752 p. (data from p.  
440 481). ISBN 5-86656-113-1. [http://elib.biblioatom.ru/text/krupnye-radiatsionnye-avarii\\_2001/go\\_0](http://elib.biblioatom.ru/text/krupnye-radiatsionnye-avarii_2001/go_0), 2001.

441 Begichev, S. N., Borovoy, A.A., Burlakov, E.V., Gavrilov, S.L., Dovbenko, A.A., Levina, L.A., Markushev, V.M.,  
442 Marchenko, A.E., Stroganov, A.A., Tataurov, A.L. Preprint IAE-5268/3: Reactor Fuel of Unit 4 of the Chernobyl NPP (a  
443 brief handbook). Kurchatov In st. Atomic Energy, 1990.

444 Beresford, N.A., Gaschak, S., Barnett, C.L., Maksimenko, A., Guliaichenko, E., Wells, C., Chaplow, J.S. A 'Reference Site'  
445 in the Chernobyl Exclusion Zone: radionuclide and stable element data, and estimated dose rates NERC-Environmental  
446 Information Data Centre. <https://doi.org/10.5285/ae02f4e8-9486-4b47-93ef-e49dd9ddec4>, 2018.

447 Beresford, N.A., Scott, E.M., Copplestone, D. Field effects studies in the Chernobyl Exclusion Zone: Lessons to be learnt J.  
448 Environ. Radioact. <https://doi.org/10.1016/j.jenvrad.2019.01.005>, 2019

449 Bondar Yu. Field studies in the Chernobyl exclusion zone along the Belarusian border (dosimetric monitoring and soil  
450 radiation analysis). Report of Polesye State Radiation and Ecological Reserve. Belarus, Khoiinki, 2015.

451 Chaplow, J. S., Beresford, N. A., and Barnett, C. L.: Post-Chernobyl surveys of radiocaesium in soil, vegetation, wildlife and  
452 fungi in Great Britain, Earth Syst. Sci. Data, 7, 215–221, <https://doi.org/10.5194/essd-7-215-2015>, 2015.

453 De Cort, M., Dubois, G., Fridman, Sh. D., Germenchuk, M. G., Israel, Yu. A., Janssens, A., Jones, A. R., Kelly, G. N.,  
454 Kvasnikova, E. V., Matveenko, I., Nazarov, I. M., Pokumeiko, Yu. M., Sitak, V. A., Stukin, E. D., Tabachny, L. Ya.,  
455 Tsaturov, Yu. S., and Avdyushin, S. I.: Atlas of caesium deposition on Europe after the Chernobyl accident, Luxembourg,  
456 Office for Official Publications of the European Communities, ISBN 92-828-3140-X, 1998.

457 Eckerman K.F. and Ryman J.C. External exposure to radionuclides in air, water, and soil. Federal guidance report No. 12,  
458 EPA-402-R-93-081, Oak Ridge National Laboratory, Tennessee 37831, USA, 238 P., 1993.

459 Fuller, N., Smith, J.T., Ford, A.T. Effects of low-dose ionising radiation on reproduction and DNA damage in marine and  
460 freshwater amphipod crustaceans. NERC Environmental Information Data Centre. <https://doi.org/10.5285/b70afb8f-0a2b-40e6-aecc-ce484256bbfb>, 2018.

462 Gaschak, S.P., Beresford, N.A., Barnett, C.L.; Wells, C., Maksimenko, A., Chaplow, J.S. 2018 Radionuclide data for  
463 vertebrates in the Chernobyl Exclusion Zone NERC-Environmental Information Data Centre.  
464 <https://doi.org/10.5285/518f88df-bfe7-442e-97ad-922b5aef003a>, 2018.

465 Hilpert K., Odoj R., and Nurnberg H. W. Mass spectrometric study of the potential of Al203/SiO2 additives for the retention  
466 of cesium in coated particles. Nucl. Technol., 61: 71, 1983.

467 IAEA. International Chernobyl Project: Technical Report. International Advisory Committee. Vienna, 1991.

468 IAEA. International Chernobyl project, technical report. ISBN 92-0-400192-5 ([http://www-pub.iaea.org/MTCD/publications/PDF/Pub886\\_web/Start.pdf](http://www-pub.iaea.org/MTCD/publications/PDF/Pub886_web/Start.pdf)), 1992.

470 IAEA. Environmental consequences of the Chernobyl accident and their remediation: twenty years of experience. Report of  
471 the Chernobyl Forum Expert Group “Environment” (eds. L. Anspaugh and M. Balonov). Radiological assessment reports  
472 series, IAEA, STI/PUB/1239, 166 pp., 2006.

473 IAEA. Guidelines on soil and vegetation sampling for radiological monitoring. Technical Reports Series No. 486.  
474 International Atomic Energy Agency. Vienna, 247p. [https://www.iaea.org/publications/12219/guidelines-on-soil-and-vegetation-sampling-for-radiological-monitoring](https://www.iaea.org/publications/12219/guidelines-on-soil-and-475-vegetation-sampling-for-radiological-monitoring). 2019.

476 Izrael, Yu.A., Vakulovsky, S.M., Vetrov, V.A., Petrov, V.N., Rovinsky, F.Ya., Stukin, E.D.. Chernobyl: Radioactive  
477 Contamination of the Environment. Gidrometeoizdat publishers, Leningrad, 223 pp. 1990 (in Russian).

478 Kashparov, V. A.: Hot Particles at Chernobyl, Environ. Sci. Pollut. R., 10, 21–30, 2003.

479 Kashparov, V. A., Ivanov, Y. A., Zvarich, S. I., Protsak, V. P., Khomutinin, Y. V., Kurepin, A. D., and Pazukhin, E. M.:  
480 Formation of Hot Particles During the Chernobyl Nuclear Power Plant Accident, Nucl. Technol., 114, 246–253, 1996.

481 Kashparov, V.A.; Lundin, S.M.; Zvarich, S.I.; Yoschenko, V.I.; Levchuk, S.E., Khomutinin, Yu.V., Maloshtan, I.N.,  
482 Protsak, V.P. Territory contamination with the radionuclides representing the fuel component of Chernobyl fallout. The  
483 Science of the Total Environment. 317(1-3), 105-119. [https://doi.org/10.1016/S0048-9697\(03\)00336-X](https://doi.org/10.1016/S0048-9697(03)00336-X), 2003.

484 Kashparov, V., Levchuk, S., Zhurba, M., Protsak, V., Khomutinin, Y., Beresford, N. A., and Chaplow, J. S.: Spatial datasets  
485 of radionuclide contamination in the Ukrainian Chernobyl Exclusion Zone, NERC-Environmental Information Data Centre,  
486 <https://doi.org/10.5285/782ec845-2135-4698-8881-b38823e533bf>, 2017.

487 Kashparov, V.; Levchuk, S.; Zhurba, M.; Protsak, V.; Khomutinin, Yu.; Beresford, N.A.; Chaplow, J.S. Spatial datasets of  
488 radionuclide contamination in the Ukrainian Chernobyl Exclusion Zone. Earth System Science Data (ESSD). 10, 339-353.  
489 <https://doi.org/10.5194/essd-10-339-2018>, 2018.

490 Kashparov, V.; Levchuk, S.; Zhurba, M.; Protsak, V.; Beresford, N.A.; Chaplow, J.S. Spatial radionuclide deposition data  
491 from the 60 km radial area around the Chernobyl nuclear power plant, 1987. NERC Environmental Information Data Centre.  
492 <https://doi.org/10.5285/a408ac9d-763e-4f4c-ba72-73bc2d1f596d>, 2019.

493 Kendrick, P., Barçante, L., Beresford, N.A., Gashchak, S., Wood, M.D. Bird Vocalisation Activity (BiVA) database:  
494 annotated soundscapes from the Chernobyl Exclusion Zone. NERC Environmental Information Data Centre.  
495 <https://doi.org/10.5285/be5639e9-75e9-4aa3-afdd-65ba80352591>, 2018.

496 Kuriny, V. D., Ivanov, Y. A., Kashparov, V. A., Loschilov, N. A., Protsak, V. P., Yudin, E. B., Zhurba, M. A., and  
497 Parshakov, A. E.: Particle associated Chernobyl fall-out in the local and intermediate zones, Ann. Nucl. Energy, 20, 415–  
498 420, 1993.

499 Lerebours, A., Smith, J.T.. Water chemistry of seven lakes in Belarus and Ukraine 2014 to 2016. NERC Environmental  
500 Information Data Centre. <https://doi.org/10.5285/b29d8ab8-9aa7-4f63-a03d-4ed176c32bf3>, 2019.

501 Loshchilov, N. A., Kashparov, V. A., Yudin, Y. B., Protsak, V. P., Zhurba, M. A., and Parshakov, A. E.: Experimental  
502 assessment of radioactive fallout from the Chernobyl accident, Sicurezza e Protezione, 25–26, 46–49, 1991.

503 Muikku, M., Beresford, N.A., Garnier-Leplace, J., Real, A., Sirkka, L., Thorne, M., Vandenbroucke, H., Willrodt, C.  
504 Sustainability and integration of radioecology—position paper J. Radiol. Prot. 38, 152-163,  
505 <http://iopscience.iop.org/article/10.1088/1361-6498/aa9c0b>, 2018.

506 National Report of Ukraine. Twenty-five Years after Chornobyl Accident: Safety for the Future. – K.: KIM. – 328 p., 2011.

507 Pontillon, Y; Ducros, G; Malgouyres, P.P. 2010. Behaviour of fission products under severe PWR accident conditions  
508 VERCORS experimental programme—Part 1: General description of the programme. Nuclear Engineering and Design.  
509 240(7), 1843–1852 <https://doi.org/10.1016/j.nucengdes.2009.06.028>, 2010.

510 Saji G. A scoping study on the environmental releases from the Chernobyl accident (part I): Fuel particles. American  
511 Nuclear Society International Topical Meeting on Probabilistic Safety Analysis, PSA 05: 685-696, 2005.

512 Salbu, B., Krekling, T., Oughton, D.H., Ostby, G., Kashparov, V.A., Brand, T.L., Day, J.P. Hot Particles in Accidental  
513 Releases from Chernobyl and Windscale Nuclear Installations. Analyst 119: 125-130, 1994.

514 Talerko N.. Mesoscale modelling of radioactive contamination formation in Ukraine caused by the Chernobyl accident. J. of  
515 Env. Radioactivity. – 78: 311-329, 2005

516 UIAR: The map of the 30-km Chernobyl zone terrestrial density of contamination with cesium-137 (in 1997), UIAR, Kyiv,  
517 Ukraine, 1998.

518 United Nations Scientific Committee on the Effects of Atomic Radiation, UNSCEAR, Sources and effects of ionizing  
519 radiation. Report to the General Assembly with Scientific Annexes, volume II, Annex D. Health effects due to radiation  
520 from the Chernobyl accident. United Nations, New York, 178 pp., 2008.

521  
522  
523  
524  
525  
526  
527  
528  
529  
530  
531  
532  
533  
534  
535  
536  
537  
538  
539  
540  
541  
542  
543  
544  
545  
546  
547  
548  
549  
550  
551

552 Appendix 1. A detailed explanation of the column headings and units (where applicable) which  
 553 accompanies the data (Kashparov et al., 2019).

554

Column_heading	Explanation	Units
Identifier	Unique identification number	not applicable
Angle_degree	A number between 10 and 360 indicates the direction from the ChNPP in degrees; 90 degrees is due east, 180 degrees is due south, 270 degrees is due west and 0/360 degrees is due north. See Figure 1.	degree
Distance_from_ChNPP_km	Distance from the Chernobyl Nuclear Power Plant (ChNPP) reactor number 4 in kilometres	kilometres
Date_gamma_measurement	Date of gamma measurement. An empty cell indicates a network point located in a water body where sample collection was not possible	dd-month-yyyy
Exposure_dose_rate_mR/h	Dose rate in air at a height of 1 metre	milliroentgen per hour
Absorbed_dose_rate_microGray/h	Absorbed dose rate is the energy deposited in matter by ionizing radiation per unit mass	Micro Gray per hour
Zr-95_Bqm <sup>2</sup>	Density of soil contamination with zirconium-95	Becquerel per square metre
Zr-95_relative_error	Relative uncertainty in determination of Zr-95 (at 68% confidence interval)	percentage
Nb-95_Bqm <sup>2</sup>	Density of soil contamination with niobium-95	Becquerel per square metre
Nb-95_relative_error	Relative uncertainty in determination of Nb-95 (at 68% confidence interval)	percentage
Ru-106_Bqm <sup>2</sup>	Density of soil contamination with ruthenium-106	Becquerel per square metre
Ru-106_relative_error	Relative uncertainty in determination of Ru-106 (at 68% confidence interval)	percentage
Cs-134_Bqm <sup>2</sup>	Density of soil contamination with caesium-134	Becquerel per square metre

Cs-134_relative_error	Relative uncertainty in determination of Cs-134 (at 68% confidence interval)	percentage
Cs-137_Bqm <sup>2</sup>	Density of soil contamination with caesium-137	Becquerel per square metre
Cs-137_relative error	Relative uncertainty in determination of Cs-137 (at 68% confidence interval)	percentage
Ce-144_Bqm <sup>2</sup>	Density of soil contamination with cerium-144	Becquerel per square metre
Ce-144_relative_error	Relative uncertainty in determination of Ce-144 (at 68% confidence interval)	percentage
Exch_Cs-134+Cs-137_Bqm <sup>2</sup>	Density of soil contamination with the exchangeable form of caesium	Becquerel per square metre
Note on empty cells	An empty cell means that data is not available	
Instrument	Gamma spectrometer with a semiconductor detector GEM-30185 ORTEC (results reported at 68% confidence level)	

555

556 Appendix 2. Decay radiation information from the master library, integrated in spectrum  
 557 analysing software tool Gelicam (EG&G ORTEC, USA), used in gamma-analyses. Activities  
 558 of <sup>106</sup>Ru and <sup>137</sup>Cs in samples were estimated via their gamma radiation emitting progenies  
 559 <sup>106</sup>Rh and <sup>137m</sup>Ba, respectively

560

Target radionuclide	Measured radionuclide	Energy, keV	Emission probability %	Half life of target radionuclides
<sup>95</sup> Zr	95Zr	724.20 756.72	44.10 54.50	64.02 days
<sup>95</sup> Nb	95Nb	765.79	99.79	34.97 days
<sup>106</sup> Ru	106Rh	621.84 1050.47	9.812 1.73	368.2 days
<sup>134</sup> Cs	134Cs	604.70 795.85	97.56 85.44	753.1 days
<sup>137</sup> Cs	137mBa	661.66	85.21	30.174 years
<sup>144</sup> Ce	144Ce	133.54	10.8	284.3 days

561